EUROPEAN ORGANIZATION FOR NUCLEAR RESEARCH

CERN-EP-2000-058
28 January 2000

A study of the angular resolution of the ALICE HMPID CsI-RICH detector

A. Di Mauro

CERN-EP/AIT

Abstract

In this report is presented an investigation of the Cherenkov angle resolution σ_{θ_c} achievable in the High Momentum Particle Identification (HMPID) CsI-RICH detector of ALICE. Two angle reconstruction procedures are described and the single contributions affecting the resolution are evaluated through the analytical treatment and the Monte Carlo simulation program *RICHSIM*. The σ_{θ_c} dependence on various detector parameters, namely the radiator thickness, the proximity gap thickness and the chamber gain, has been studied carrying out beam tests of CsI-RICH prototypes. A ring resolution of about 2 mrad has been achieved, for β=1 particles, in the optimal detector configuration (10 mm C_6F_{14} radiator thickness, 103 mm proximity gap and 40 ADC channels single electron average pulse height).

1 Introduction.

The High Momentum Particle Identification (HMPID) RICH detector of ALICE is devoted to the detection of π, K and p in the 1 to 5 GeV/c momentum range. It has a proximity focusing geometry and consists of a 10 mm liquid C_6F_{14} radiator, contained by a 5 mm quartz window and separated by a 103 mm gap (filled with CH_4) from the Cherenkov photon detection plane, which is a CsI photocathode segmented into pads for two-dimensional readout. Detailed descriptions of the HMPID detector and of the test-beam setup (used to assess the performance of several prototypes) are given in [1, 2, 3].

Here is presented a detailed study of the Cherenkov angle resolution achieved in single particle test-beam events, based on the estimation of the single contributions to the resolution via the Monte Carlo simulation program *RICHSIM* (described in [1]) and the analytical calculation.

2 Angle reconstruction algorithms and analytical treatment.

The Cherenkov angle is affected by the following errors:

(1) The *chromatic error*, related to the variation of the radiator refractive index n with the photon energy E. It is generated by the dispersion dn/dE of the radiator medium index and by the spread of the detector response over the effective photon energy range. The detector response, in turn, is determined by the convolution of the CsI photocathode (PC) quantum efficiency (QE) with the transmission of the media traversed by the Cherenkov photons inside the detector: 10 mm liquid C_6F_{14} radiator, 5 mm quartz window and about 100 mm of gas mixture, basically composed by CH_4, occasionally with a small percentage of i-C_4H_{10} and few ppm's of oxygen and water vapour pollutant. (fig. 1).

(2) The *geometric error*, related to the spread of the emission point along the particle path in the Cherenkov radiator. It depends on the ratio T_r/T_g between the radiator thickness, T_r, and the proximity gap thickness, T_g; it can be minimized mainly by increasing T_g since a reduction of T_r will decrease the number of Cherenkov photons per ring and therefore the pattern recognition capability.

(3) The *localization error*, related to the precision with which the photon and particle impact coordinates can be measured. It is determined by the photodetector geometry (pad size, sense wires pitch) and by the photon feedback.

(4) The track *incidence angle error*, related to the particle angle θ_p and to the precision of the tracking devices.

While the chromatic and geometric error are intrinsic, respectively, to the radiator properties and to the proximity focusing technique the last two are determined by experimental conditions, like the photodetector gain A_0 and the tracking quality.

The reconstruction of the Cherenkov angle θ_c is obtained through a transformation of the measured ring radius R. Then, from the resulting functional dependence, $\theta_c = \theta_c(R, E, T_r, \theta_p)$, the spread of the reconstructed Cherenkov angle distribution can be analytically estimated as:

$$\sigma_{\theta_c} = [\sum_{i=1}^{4} (\frac{\partial \theta_c}{\partial v_i} \sigma_{v_i})^2]^{1/2}, \tag{1}$$

where the variables v_i are: E, T_r, R, θ_p and σ_{v_i} are the respective rms errors.

Two methods have been used for the Cherenkov angle reconstruction, in real and simulated events. The first one, the *loop-method*, is based on the search of the best angle through an iterative procedure described in [4]. The other, called β*-method*, is a simple transformation of the Cherenkov ring radius based on the knowledge of the particle β which eliminates the direct analytical dependence on n. Since the photon *emission point* in the radiator, X_{ep} and the photon

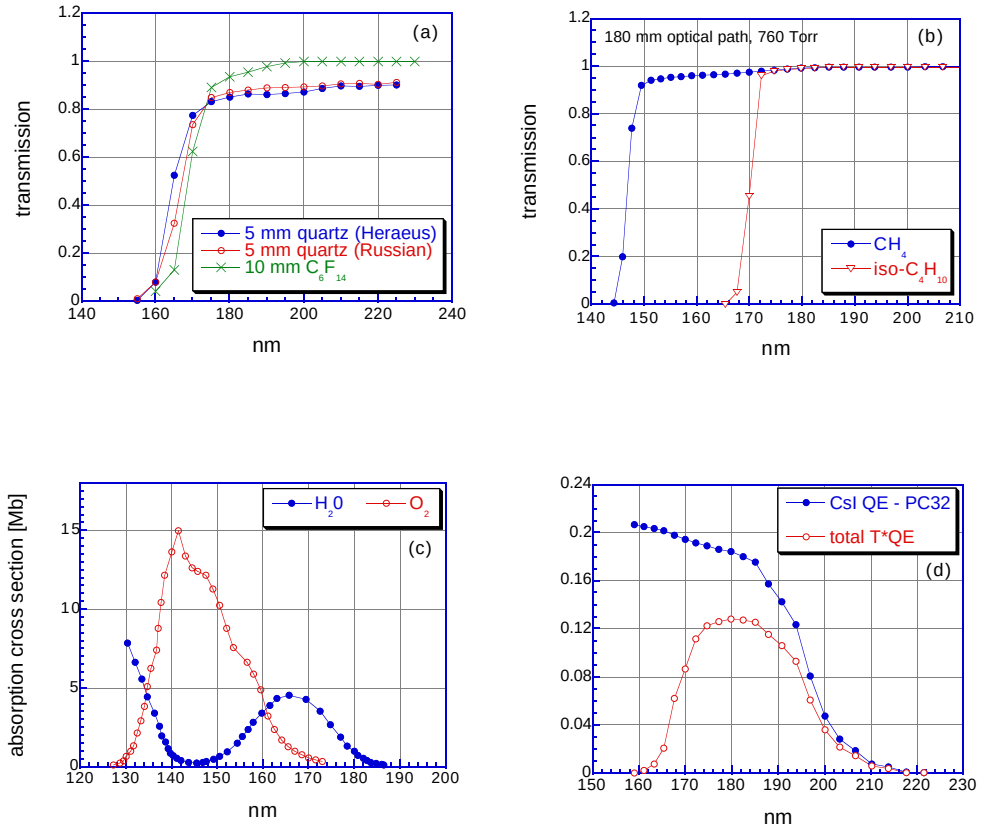

Figure 1: (a) Measured UV transmission of 10 mm C_6F_{14} and 5 mm quartz plates, supplied by two different companies. (b) UV transmission of CH_4 and i-C_4H_{10}, calculated from [5] and [6] respectively, for a photon path of 180 mm equivalent to a distance traveled in a proximity gap of 103 mm by Cherenkov photons emitted in C_6F_{14} by $\beta = 1$ particles. (c) UV absorption cross section of oxygen [7] and water vapour [8]. (d) photocathode PC32 QE evaluated from test-beam data and the convolution with the total transmission.

energy are unknown, in both methods, the angle reconstruction has been achieved by fixing them at the most probable values. In particular, X_{ep} is about 5.2 mm for perpendicular tracks in a 10 mm radiator; it is not at the radiator centre since photons generated in the first radiator half have larger probability of beeing absorbed due to the longer path in the C_6F_{14}). The average energy E_{av} is 181 nm (6.85 eV) over the detector response (fig. 1d).
Fig. 2 shows the single photon experimental distributions of ring radius and the corresponding reconstructed Cherenkov angle distributions, either single photon or ring averaged (with $\sigma_{\theta_c}^{ring} \sim \frac{\sigma_{\theta_c}^{single}}{\sqrt{N_{phot}}}$), obtained by means of the two mentioned procedures. The β algorithm provides, of course, the best resolution; however its application to the analysis of real multi-particle events needs either a pre-filtering by a general method estimating the β associated to each considered particle or a probability table allowing to test the hypothesis concerning the possible kind of particle.

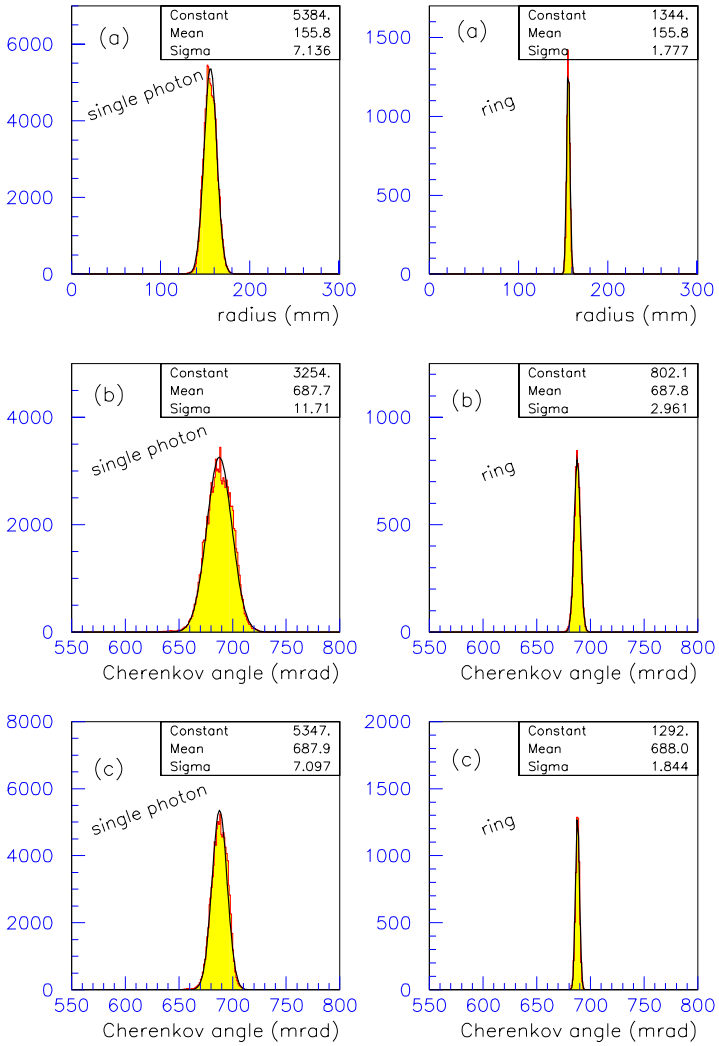

Figure 2: Single photon and ring averaged, radius distributions (a) and Cherenkov angle distributions from: (b) the *loop-method* and (c) the β*-method.* Experimental data from SPS test-beam (350 GeV/c π), PC32, chamber gain $A_0 \sim 40$ ADC channels (1 ADC = 0.17 fC).

2.1 The *loop-method.*

In the first step, the angle ϕ_c, defined by the plane containing the particle trajectory and the photon impact, is calculated and, assuming $\theta_c = \theta_c(E_{av})$ and β = 1, photon tracking is executed starting from X_{ep} through the media up to the CsI PC, producing an impact point at a distance Δs from the measured point of coordinates (x_c, y_c). Then a new tracking is started after having increased θ_c and ϕ_c by $(\mathrm{d}\theta_c/\mathrm{d}s)\Delta s$ and $(\mathrm{d}\phi_c/\mathrm{d}s)\Delta s$ respectively, with the derivatives evaluated with a 0.5 mrad variation of each angle. The condition which stops the iteration is $\Delta s \leq 0.1$ mm, a value which is much smaller than the spatial resolution of 2 mm estimated for the photodetector and resulting from the photon feedback [1].
A vector ray trace with refraction at all surfaces in the detector media gives the following equation for the photon coordinates [9]:

$$x_c = Ra_x, \tag{2}$$

$$y_c = Ra_y, \tag{3}$$

where

$$R = \frac{T_r}{a_z} + \frac{T_q}{\sqrt{a_z^2 + (\frac{n_q}{n})^2 - 1}} + \frac{T_g}{\sqrt{a_z^2 + (\frac{1}{n})^2 - 1}}. \quad (4)$$

T_r, T_q and T_g are the thicknesses of radiator, quartz window and proximity gap, respectively; a_x, a_y, a_z are the photon direction cosines in the detector reference system. In the limit case $T_r, T_q \to 0$, an explicit solution giving θ_c as a function of the measured quantities (x_c, y_c, θ_p) is obtained:

$$cos\theta_c = cos\phi_p sin\theta_p a_x + sin\phi_p sin\theta_p a_y + cos\theta_p a_z, \quad (5)$$

with ϕ_p particle track azimuthal angle, $a_x = x_c/nr$, $a_y = y_c/nr$, $a_z = \sqrt{1 - \frac{x_c^2+y_c^2}{n^2 r^2}}$ and $r^2 = x_c^2 + y_c^2 + T_g^2$. Thus, the explicit dependence on x_c, y_c, θ_p allows to evaluate directly the localization and incidence angle contributions:

$$\frac{\partial\theta_c}{\partial x_c} = \frac{\beta k^{1/2}}{T_g \alpha}[k(cos\phi' cos\phi_p - cos\theta_p sin\phi' sin\phi_p) - \frac{\alpha\mu}{\beta^2} sin\theta_p sin\phi'], \quad (6)$$

$$\frac{\partial\theta_c}{\partial y_c} = \frac{\beta k^{1/2}}{T_g \alpha}[k(cos\phi' sin\phi_p + cos\theta_p sin\phi' cos\phi_p) + \frac{\alpha\epsilon}{\beta^2} sin\theta_p sin\phi'], \quad (7)$$

$$\frac{\partial\theta_c}{\partial\theta_p} = -cos\phi', \quad (8)$$

where $k = 1 - n^2 + \frac{\alpha^2}{\beta^2}$, $\phi' = \phi_c - \phi_p$ and ϵ, μ, α are the photon direction cosines in the system of the particle:

$$\epsilon = sin\theta_p cos\phi_p + tan\theta_c(cos\theta_p cos\phi' cos\phi_p - sin\phi' sin\phi_p), \quad (9)$$

$$\mu = sin\theta_p sin\phi_p + tan\theta_c(cos\theta_p cos\phi' sin\phi_p + sin\phi' cos\phi_p), \quad (10)$$

$$\alpha = cos\theta_p - tan\theta_c cos\phi' sin\theta_p. \quad (11)$$

Finally, the chromatic and geometric contributions have to be calculated considering the implicit dependence of θ_c on n and L through the measured variables x_c, y_c :

$$\frac{\partial\theta_c}{\partial n} = \frac{cos\theta_p}{\alpha}\frac{n^2\beta^2}{ntan\theta_c}, \quad (12)$$

$$\frac{\partial\theta_c}{\partial T_r} = (\frac{1}{1 + \frac{\epsilon_{T_r} k}{\alpha^2 cos^2\theta_c}})(\frac{\beta k^{3/2} tan\theta_c \lambda}{T_g \alpha^2} + \frac{1 + \epsilon_{T_r} k\beta^2}{\alpha^2(1 + \epsilon_{T_r})}\frac{k^{1/2} tan\theta_c}{T_g \beta}(1 - \lambda)), \quad (13)$$

where

$$\epsilon_{T_r} = \frac{T_r - X_{ep}}{T_g}\frac{\beta k^{1/2}}{\alpha}, \quad (14)$$

$$\lambda = 1 - sin^2\theta_p sin^2\phi_c. \quad (15)$$

2.2 The β-*method.*

Fig. 3 illustrates the geometry for the angle reconstruction with perpendicular incidence particles; in the case of oblique tracks an image correction through a detector rotation is needed. The measured ring radius R can be expressed as:

$$R = \Delta R_{rad} + \Delta R_{qz} + R_o, \tag{16}$$

where $\Delta R_{rad} = (T_r - X_{ep}) \cdot tan\theta_c(E_{av})$ and $\Delta R_{qz} = T_q tan\theta_{qz}(E_{av})$ are constant terms and $R_o = T_g \cdot tan\theta_o$. θ_o can be simply expressed as a function of θ_c by means of Snell's law; then, assuming the refractive index of the gas medium in the proximity gap equal to 1, we get:

$$R_o = T_g \frac{nsin\theta_c}{\sqrt{1 - n^2 sin^2\theta_c}}. \tag{17}$$

Using the Cherenkov relation, $cos\theta_c = \frac{1}{n\beta}$, in the previous expression, the following equation

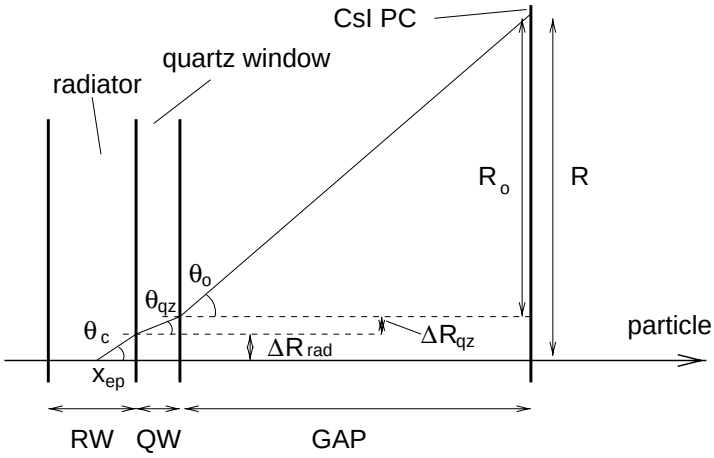

Figure 3: Cherenkov photon optical path through the detector and geometry for the β-*method* angle reconstruction.

is obtained:

$$n = \sqrt{\frac{1}{1 + \frac{T_g^2}{R_o^2}} + \frac{1}{\beta^2}}, \tag{18}$$

which can in turn be put in the Cherenkov relation to calculate the angle as:

$$\theta_c = acos\left(\frac{1}{\sqrt{\frac{\beta^2}{1+\frac{T_g^2}{R_o^2}} + 1}}\right), \tag{19}$$

where T_g and the β of the particle are known and R_o can be deduced from the measured radius R through the relation (16).
In this case θ_c depends, directly, only on R; then the localization contribution to the resolution will be simply:

$$\frac{\partial\theta_c}{\partial R} = \frac{\partial\theta_c}{\partial R_o} = \frac{cos^2\theta_c}{tan\theta_c}\beta^2 \frac{T_g^2 R_o}{(T_g^2 + R_o^2)^2}. \tag{20}$$

To find the errors associated to the remaining variables, it is needed to estimate the variation of R with the same variables and finally calculate $(\partial\theta_c/\partial v_i)$ using the following expression:

$$\frac{\partial\theta_c}{\partial v_i} = \frac{\partial\theta_c}{\partial R}\frac{\partial R}{\partial v_i}. \tag{21}$$

The result is:

$$\frac{\partial R}{\partial n} = (T_r - X_{ep})\frac{n\beta^2}{tan\theta_c} + T_q\frac{n}{n_q h^2}\frac{1}{(\frac{1}{h} - \frac{1}{n_q^2})^{3/2}} + T_g\frac{n}{h^2}\frac{1}{(\frac{1}{h} - 1)^{3/2}}, \tag{22}$$

$$\frac{\partial R}{\partial T_r} = tan\theta_c, \tag{23}$$

where $h = \frac{1}{n^2 - \frac{1}{\beta^2}}$ and n_q is the quartz refractive index.
The contribution of the particle track polar and azimuthal angles, θ_p and ϕ_p respectively, can be evaluated by considering the following relation:

$$\frac{\partial\theta_c}{\partial\theta_p} = \frac{\partial\theta_c}{\partial R}\frac{\partial R}{\partial a_z}\frac{\partial a_z}{\partial\theta_p}, \tag{24}$$

and a similar one for ϕ_p. Here the variables R and a_z are those defined in the *loop* algorithm; indeed in the case of oblique tracks the ring image is tranformed through a detector rotation, according to the photons polar and azimuthal angles in the proximity gap reconstructed by the *loop-method*. In the limit case $T_r, T_q \to 0$, the resulting contributions are:

$$\frac{\partial\theta_c}{\partial\theta_p} = -cos(\phi_c - \phi_p) \tag{25}$$

and

$$\frac{\partial\theta_c}{\partial\phi_p} = -sin\theta_p sin(\phi_c - \phi_p). \tag{26}$$

2.3 Evaluation of the rms errors.

The final step of the analytical treatment is the evaluation of the rms errors σ_{v_i} to be used in the relation (1). Such quantities are strictly related to the detector response, while the partial derivatives listed above represent a general feature of the proximity focusing configuration.
The evaluation of the chromatic rms error, $\sigma_E = (dn/dE)\sigma_E^{det}$, was shown to be very crucial to reproduce the measured angular resolution, either with *RICHSIM* or by means of the analytical treatment. The parameter dn/dE is a physical property of the liquid radiator. The first measurement of the C_6F_{14} refractive index, from J. Seguinot [8], was limited to the range from 195 to 250 nm and the experimental data were best fit with $n(E) = a + b \cdot E$ with $a = 1.2177$ and $b = dn/dE = 0.00928$ eV^{-1} (fig. 4). Such a curve does not reproduce our test beam data: at the average wavelength of detected Cherenkov photons of 181 nm (fig. 1d) the index is 1.28127, a value corresponding to a ring radius of 144.5 mm (for β = 1 particles and a proximity gap of 103 mm), instead of the observed 156 mm (fig. 2a). The value needed to obtain the right ring radius (and to reconstruct correctly the Cherenkov angle) is $n = 1.2948$, at the average detected photon wavelength. The index dispersion has been adjusted in order to get, in Monte Carlo events, the correct spread in the distributions of either the ring radius and the reconstructed Cherenkov angle. Indeed a and b have been estimated with a trial and error method, taking into account all the tunable parameters (namely the photon feedback rate and the CsI quantum efficiency). The

values giving the best fit to data are: $a = 1.177$ and $b = 0.0172$ eV^{-1}. The corresponding curve is also shown in fig. 4, together with the recent DELPHI measurements (data by courtesy of E. Fokitis, S. Maltezos and P.G. Moyssides [10]). Although they refer to two different temperatures (27.5 ^{o}C for DELPHI and 22.5 ^{o}C for the HMPID *RICHSIM*), the two sets of data are in good agreement, since the experimental error quoted for the DELPH index corresponds to an uncertainty of about 4 ^{o}C, according to the temperature coefficient $dn/dT = -5 \times 10^{-4}$ ^{o}C^{-1} given by the supplier.

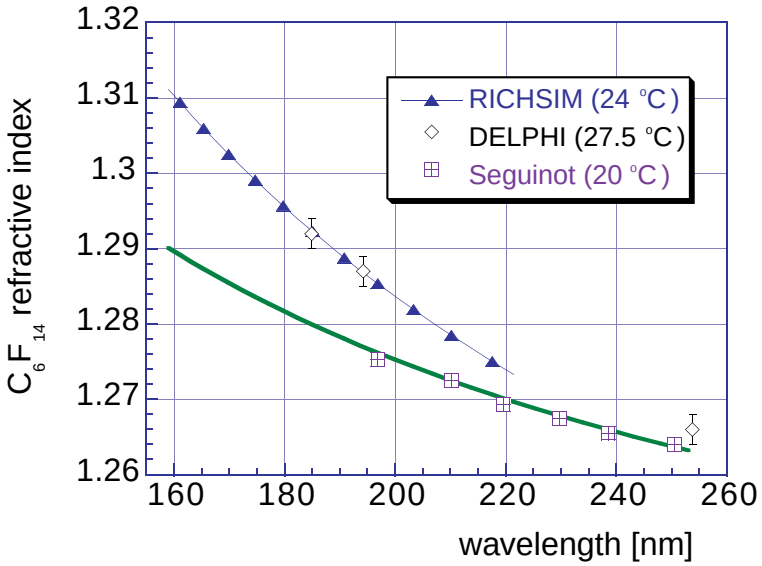

Figure 4: The C_6F_{14} refractive index. The J. Seguinot [8] and DELPHI [10] values are experimental, while the HMPID curve has been deduced to best reproduce with Monte Carlo events test beam distributions. A linear fit with $n(E) = a + b \cdot E$ is also superimposed, with a and b beeing 1.2177 and 0.00928 eV^{-1}, for J. Seguinot data, and 1.177 and 0.0172 eV^{-1}, for *RICHSIM* data.

The second factor in the σ_E expression, σ_E^{det}, represents the standard deviation of the detected Cherenkov photon spectrum resulting by the convolution of all media UV-transmission with the CsI QE (fig. 1d). The shape of that distribution suggests a triangular response of the detector to UV photons and, therefore, σ_E^{det} can be approximated by $\Delta E/\sqrt{24} = 1.8/\sqrt{24}$ eV. Finally, the resulting chromatic rms error is: $\sigma_E = 6.33 \times 10^{-4}$.
For the geometric rms error, σ_{T_r}, the calculation is straightforward: $\sigma_{T_r} = T_r/(\sqrt{12} cos\theta_p) = 2.89$ mm$/cos\theta_p$.
The total localization rms error, σ_R, includes the indeterminacy of both particle and photon x, y coordinates; it has been evaluated with the support of simulation and dedicated measurements of pad response. Along the x direction, the spatial resolution achievable with the center of gravity method is typically less than 1 mm; along the y direction, which, in our case, is perpendicular to the anode wires, the impact position can only be associated to the closest wire and, therefore, the localization error is $pitch/\sqrt{12}$. Nevertheless, the values used to calculate σ_R are $\sigma_x = 2$ mm and $\sigma_y = 2.5$ mm, either for photons or for particles, which are very close, respectively, to x and y pad size/$\sqrt{12}$ (with 8×8.4 mm pad). Indeed there are several factors contributing to

the deterioration of the spatial resolution. A first error is introduced by the finite sampling of the charge related to the detector pad segmentation [1]. Then, in the case of photons, a large fraction (∼45%) of pad clusters are made by a single pad and the centroid evaluation is not possible. Finally, the photon feedback can affect the localization accuracy, especially in the case of particles, due to the larger total charge developed.
Lastly, the particle track angles rms errors will depend on the tracking system. In the present test configuration, the ϕ_p contribution can be considered negligible while the rms error concerning θ_p has been assumed equal to 5 mrad.
Figure 5 shows the variation of the calculated contributions to the total angular resolution as a function of the angle ϕ_c, for two particle track angles θ_p, 0 (a) and 7.5 (b) degrees, respectively; the second value is the average track polar angle expected in the ALICE HMPID detector [1].

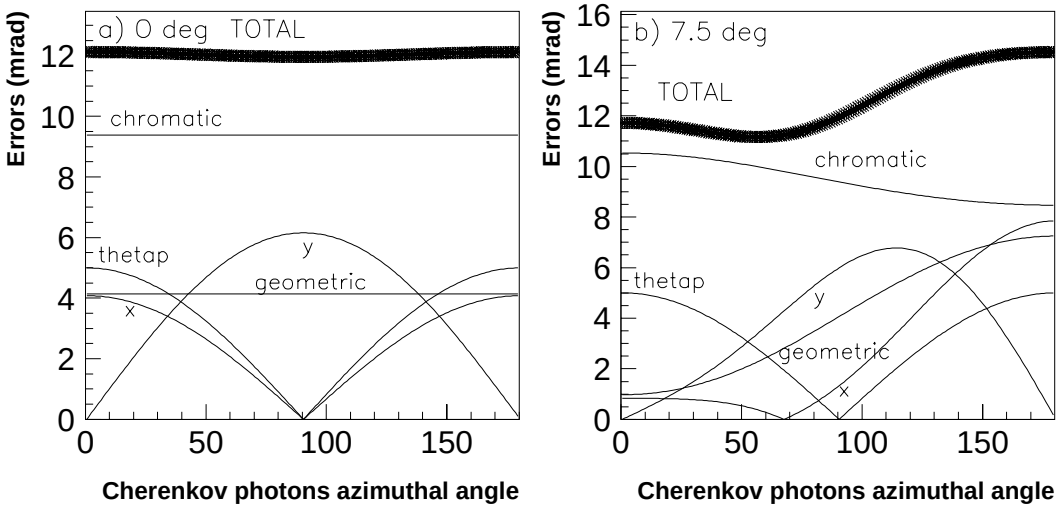

Figure 5: Variation of the contributions to the Cherenkov angle resolution, from the *loop-method*, with the photons azimuthal angle ϕ_c, at particle track angles (a)$\theta_p = 0^o$ and (b)$\theta_p = 7.5^o$.

In the following the θ_p contribution will not be quoted in tables and plots but just included in the calculation of total the angular resolution.
In table 1 are reported the results of analytical estimation of each contribution in the two methods; for comparison, the same errors have been evaluated with the Monte Carlo simulation program, described in [1]. The presented values refer to $\beta = 1$, $T_r = 10$ mm, $T_q = 5$ mm and $T_g = 103$ mm.

Error	CALCULATION		SIMULATION	
	β-method (mrad)	loop-method (mrad)	β-method (mrad)	loop-method (mrad)
chromatic	5.7	9.4	5.9	9.7
geometric	2.5	4.1	2.6	4.2
localization	3.1	4.8	3.1	5

Table 1: Single photon Cherenkov angle errors from analytical treatment and simulation.

3 Optimization of the angular resolution in beam tests.

The analytical treatment and the simulation have been developed aiming at a better understanding of experimental data and, hence, at the optimization of the detector response in terms of angular resolution. Several studies have been carried out in beam-tests, at the CERN PS and SPS, allowing to analyse, in single particle events, the angular resolution dependence on:

- the Cherenkov ring radius (proximity gap dependent),
- the chamber gain (high voltage and gas mixture dependent),
- the radiator thickness,
- the particle incidence angle θ_p.

In fig. 6 is reported the measured ring angular resolution, from the *loop-method*, as a function of the number of resolved clusters, corresponding to the reconstructed hits of Cherenkov photons. The data have been fit with a function $y = \sqrt{\frac{a}{x} + b}$, with $\sqrt{a} = 11.7$ mrad beeing very close to the single photon angular resolution and b=1 mrad^2 a parameter related to the intrinsic detector resolution.

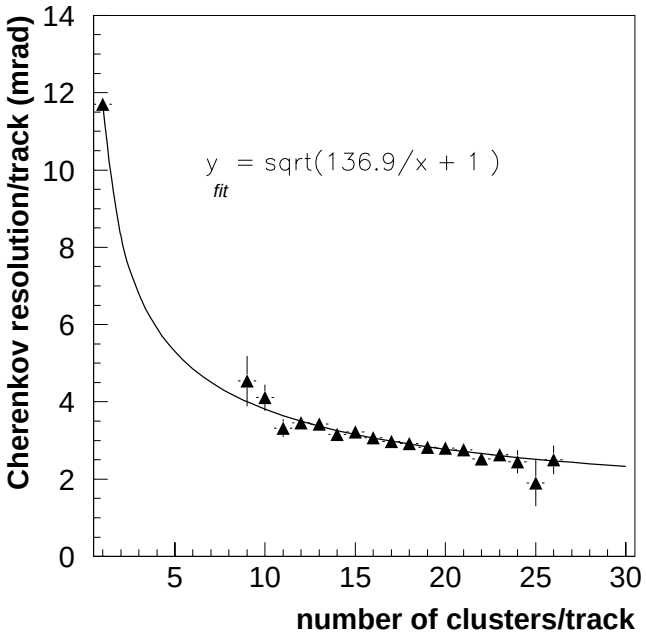

Figure 6: Ring angular resolution, from Cherenkov angles reconstructed with the *loop-method*, as a function of the number of resolved cluster per event. The superimposed curve is a fit showing the proportionality to $\frac{1}{\sqrt{N_{phot}}}$.

In fig. 7 are reported the calculated single errors ($(\partial\theta_c/\partial v_i)\sigma_{v_i}$) and the total angular resolution (σ_{θ_c}), estimated from analytical calculation, *RICHSIM* events and test-beam events, for both reconstruction algorithms, as a function of the ring radius. The results quoted in these plots point out the dominance of the chromatic error over the other contributions, especially at ring radii > 100 mm; therefore a reduction of the localization error, which could be obtained with a finer detector segmentation, would produce a only a marginal improvement of the angular resolution, not compensating the effort needed to increase the number of electronic channels. In fig. 8 are reported the single photon and ring angular resolution, from measurements and

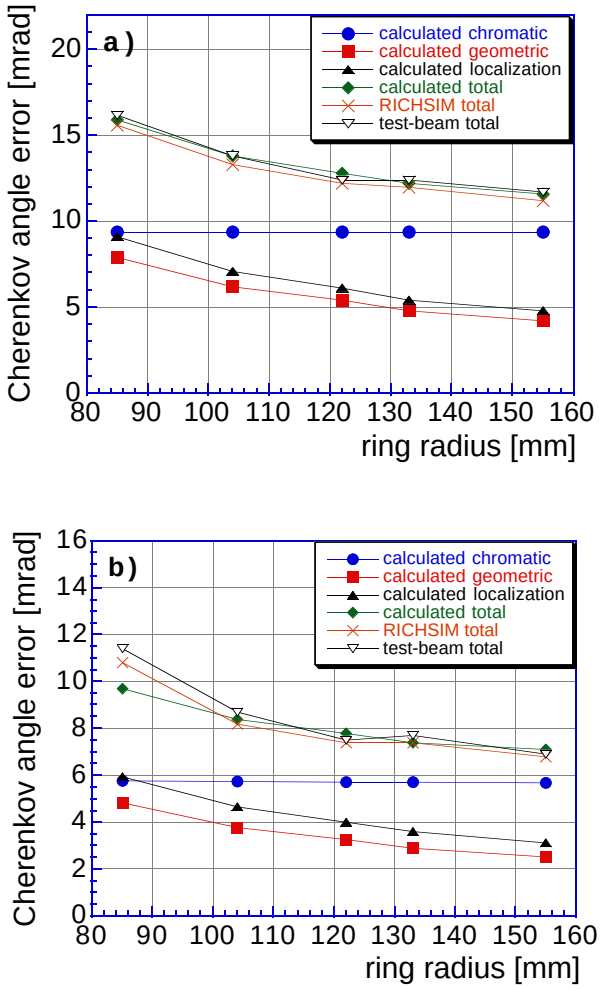

Figure 7: Single photon Cherenkov angle errors from analytical treatment and simulation, in the *loop-method* (a) and the β-*method* (b), as a function of the ring radius.

simulation, as a function of the chamber gain (represented by the single electron average pulse height A_0). The stability of the single photon σ_{θ_c} with the increase of A_0, could result by the sum of two opposite effects: the larger feedback contribution, deteriorating the resolution, and the smaller fraction of single pad clusters, improving the resolution mainly in the x direction. The deterioration of the ring angular resolution at lower A_0 values is originated by a reduced detection efficiency which decreases the number of photoelectrons. In the mixture with i-C_4H_{10} the single photon resolution is better than in pure CH_4, probably due to the lower UV-transmission of i-C_4H_{10} reducing the chromatic aberration and the photon feedback contribution; however the ring averaged resolution is similar to that in pure CH_4 because of the smaller number of Cherenkov photons determined by the presence of i-C_4H_{10} [1].

In fig. 9 are reported the single photon and ring angular resolution, from measurements and

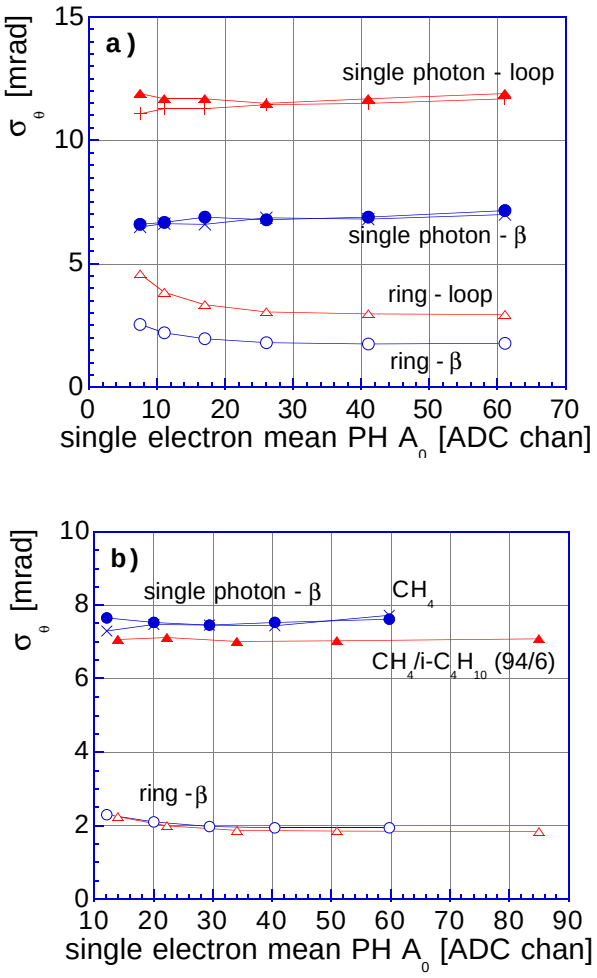

Figure 8: (a) Angular resolution, for the *loop and β-methods*, as a function of the single electron PH A_0 at $R = 155$ mm, in CH_4; circles and triangles: measurements; crosses: simulation. (b) Angular resolution, for the β-methods as a function of the single electron PH A_0 at $R = 122$ mm, in two gas mixtures; circles and triangles: measurements; crosses: simulation. SPS beam-test (350 GeV/c π), PC32.

simulation, as a function of the particle incidence angle θ_p. No significant deterioration of the resolution is observed in the range of θ_p where most of the HMPID expected tracks will fall.

Finally, fig. 10 shows the single photon and ring angular resolution, from measurements and simulation, as a function of the radiator thickness T_r. The small variations of the single photon σ_{θ_c} are related to changes of the ring radius and of the spectrum of the transmitted Cherenkov photons with T_r. As expected, the ring σ_{θ_c} worsen at smaller T_r as a consequence of the reduced number of emitted Cherenkov photons.

4 Conclusions.

The Cherenkov angle resolution of the ALICE CsI-RICH detector has been studied combining the analysis of single particle test-beam events with either the analysis of Monte Carlo events and the analytical treatment of the Cherenkov angle errors.
Two angle reconstruction algorithms have been described and for both the single contributions

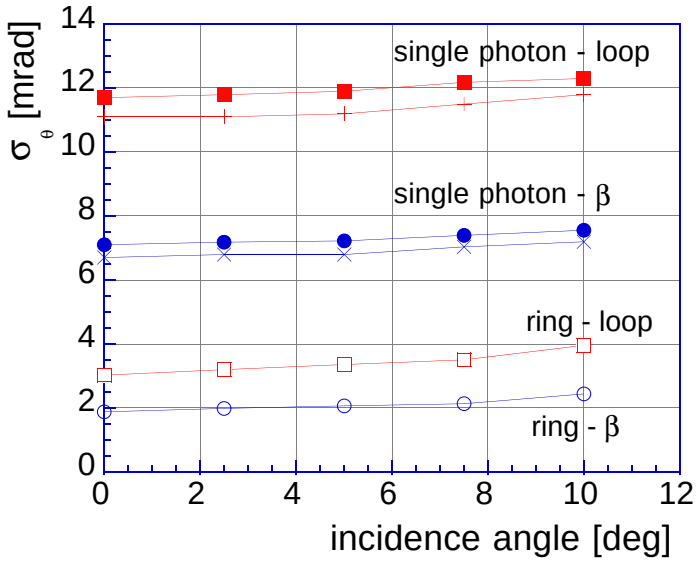

Figure 9: Angular resolution, for the *loop and β-methods*, as a function of the particle track polar angle at $A_0 \sim 40$ ADC channels and R=155 mm; circles and squares: measurements; crosses: simulation; SPS beam-test (350 GeV/c π), PC32.

to the angular resolution have been estimated via the simulation and the analytical treatment. The agreement between analytical treatment, simulation and test-beam results is very accurate in the considered detector parameters dependencies.
The *β-method* provides the best ring angle resolution (1.9 mrad with $\beta = 1$ particles, 10 mm C_6F_14 radiator and 103 mm proximity gap. However the application of such an algorithm to real multi-particle events relies on the estimation of the particle β to be used in the angle reconstruction.
The chromatic aberration is the most limiting factor in the overall Cherenkov angle resolution; hence a reduction of the geometric and localization errors will not determine a significant improvement of the angular resolution. As a consequence, basic detector parameters like the radiator thickness, the proximity gap and the PC pad size could be varied within suitable ranges in order to satisfy other requirements than the angular resolution. For example, an increase of the radiator thickness will produce a larger number of photons per ring, or a larger pad size will reduce the number of readout channels and therefore the front-end electronics costs. These and other aspects are currently under evaluation to optimize the detector design.

5 Acknowledgements.

The calculations of the individual contributions to the angle resolution have been based on the analytical treatment developed by T. Ypsilantis in [9]. I am very grateful to T. Ypsilantis for many helpful discussions.
I also warmly thank my colleagues of the HMPID group for their contribution to the experimental tests and several useful discussions.

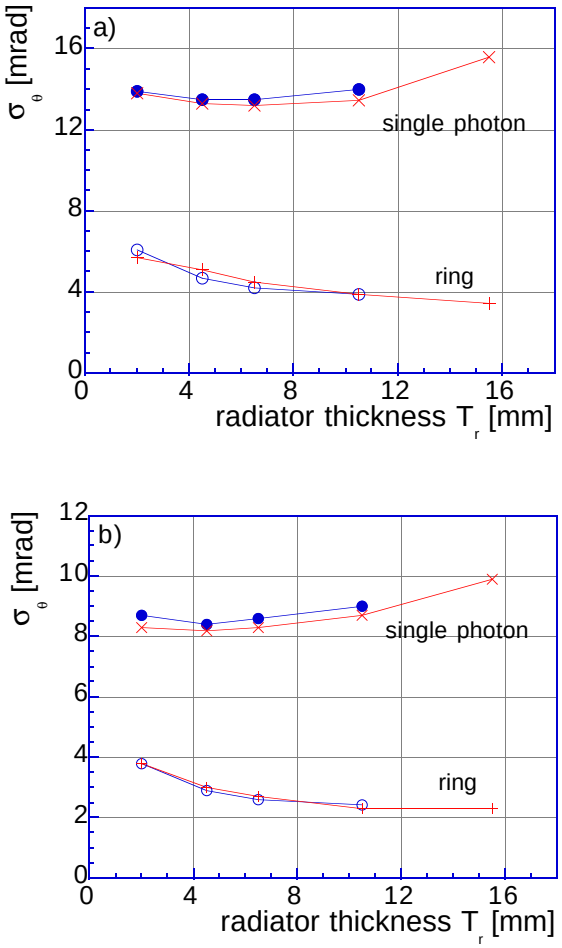

Figure 10: Angular resolution, for (a)the *loop-method* and (b) the β*-method*, as a function of radiator thickness at $A_0 \sim 40$ ADC channels and R= 104 mm; circles: measurements; crosses: simulation; PS beam-test (3 GeV/c π), PC24.

References

[1] *ALICE collaboration,* **Technical Design Report of the High Momentum Particle Identification Detector, CERN/LHCC 98-19**;

[2] *F. Piuz et al.*, **Nucl. Instr.** & **Methods A433(1999), 222**;

[3] *A. Di Mauro et al.*, **Nucl. Instr.** & **Methods A433(1999), 190**;

[4] *R. Arnold et al.*,**Nucl. Instr. & Meth. A270(1988), 289-318**;

[5] *G. H. Mount et al.*, **The Astrophysical Journal 214:L47-L49, 1977**;

[6] *C. Lu, K.T. McDonald*,**Nucl. Instr.** & **Methods A343(1994), 135**;

[7] *A. Amoruso et al.*, **J. Quant. Spectr. Radiat. Transfer Vol. 56,145 (1996)**;

[8] *J. Seguinot, "Les compteurs Cherenkov: applications et limites pour l'identification des particules"*,**Ecole J.Curie de Physique Nucleaire, Mabuisson (France) 26-30/9/1988**;

[9] *T. Ypsilantis, J. Seguinot* ,**Nucl. Instr. & Meth. A 343 (1994), 30-51**;

[10] *E. Fokitis et al.* ,**Measurements of the refractive index of DELPHI RICH radiators in liquid phase down to 185 nm**, *in preparation.*